



HAL
open science

Surface sulfation of crab chitin for anisotropic swelling and nanodispersion

Xijun Wang, Pan Chen, Xiao Feng, Chao Dang, Baofeng Lin, Yoshiharu Nishiyama, Haisong Qi

► **To cite this version:**

Xijun Wang, Pan Chen, Xiao Feng, Chao Dang, Baofeng Lin, et al.. Surface sulfation of crab chitin for anisotropic swelling and nanodispersion. *Cellulose*, 2022, 29 (13), pp.7099-7109. 10.1007/s10570-022-04688-2. hal-03746705

HAL Id: hal-03746705

<https://hal.science/hal-03746705>

Submitted on 8 Aug 2022

HAL is a multi-disciplinary open access archive for the deposit and dissemination of scientific research documents, whether they are published or not. The documents may come from teaching and research institutions in France or abroad, or from public or private research centers.

L'archive ouverte pluridisciplinaire **HAL**, est destinée au dépôt et à la diffusion de documents scientifiques de niveau recherche, publiés ou non, émanant des établissements d'enseignement et de recherche français ou étrangers, des laboratoires publics ou privés.

Surface sulfation of crab chitin for anisotropic swelling and nanodispersion

Xijun Wang,^{†,‡} Pan Chen,^{*,¶} Xiao Feng,[‡] Chao Dang,[‡] Baofeng Lin,^{*,†} Yoshiharu Nishiyama,^{*,§} and Haisong Qi^{*,‡}

[†]*School of Chemistry and Chemical Engineering, Guangxi University, Nanning 530004, China*

[‡]*State Key Laboratory of Pulp and Paper Engineering, South China University of Technology, Guangzhou, 510640, China*

[¶]*Beijing Engineering Research Centre of Cellulose and Its Derivatives, School of Materials Science and Engineering, Beijing Institute of Technology, 100081, Beijing, P.R. China*

[§]*Univ. Grenoble Alpes, CNRS, CERMAV, 38000 Grenoble, France*

E-mail: panchen@bit.edu.cn; lbf@gxu.edu.cn; yoshi@cermav.cnrs.fr; qihs@scut.edu.cn

Abstract

Crab chitin was sulfated under heterogeneous conditions using sulfamic acid in N,N-dimethylformamide (DMF) to selectively sulfate the microfibril surface. The degree of sulfation followed a first order kinetics assuming a limited available reaction sites on the surface, and leveled off at a bulk degree-of-substitution of 0.4, corresponding to 2 mol/kg of sulfate groups. The reaction rate was proportional to the square of sulfamic acid concentration, suggesting involvement of two sulfamic acid molecules in a reaction. When washed with water after sulfation, the crab shell chitin fragments swelled anisotropically in the helicoidal axis direction, revealing regular alternating birefringence under optical microscope. Further mechanical treatment with high-pressure homogenizer led

to slender nanofibrils, whose diameters were of the order of 6 nm according to turbidimetric analysis, in agreement with the Scherrer size estimated from X-ray diffraction line broadening. Both atomic force microscope (AFM) and transmission electron microscope (TEM) measurement showed presence of further smaller fragments with diameter of 3-4 nm and length of 300 nm. The current approach presents a rapid and efficient modification to chitin, and a strategy for the preparation of stable nanochitin suspension.

Keywords

Chitin, Sulfation, anisotropic swelling, nanochitin, nanodispersion

Introduction

Chitin is a linear natural polymer that consists of β -(1-4)-2-deoxy-2-N-acetamido-D-glucopyranose residues that assembles into semi-crystalline microfibrils inert to most chemicals. It usually forms complex with protein, occurring as structural components and providing mechanical support in various living organisms. Harsh treatments leads to stable colloidal suspension of elongated nanometric particles that self organize into chiral nematic structure similar to cellulose nanocrystals.¹⁻³ There is a large panel of potential application as building block of functional materials common to cellulose nanocrystals or cellulose nanofibers, but in addition, chitin also presents an advantage of being bioresorbable in animal body including human body,⁴ which can be an advantage in biomedical applications.

Nanochitin has been widely used in industry fields such as adhesive, wearable devices and superhydrophobic coating. In the beginning, simple hydrolysis using hydrochloric acid has been used to prepare nanochitin, typically at concentration of 2.5 N with reflux¹ or 3 N at 90 °C,⁵ which happens to cleave long fibrils into shorter fragments, as in the case of cellulose. For chitin, this hydrolysis process also removes labile N-acetyl groups on the

surface of crystal, while preserving the inside of crystals intact. The surface deacetylation leaves amine groups that are protonated at lower pH, leading to positive surface charge to confer colloidal stability.

One can also selectively deacetylate the crystal surface by alkali treatment. Alkali treatment using highly concentrated sodium hydroxide solutions, typically around 50%, are used to produce water soluble chitosan due to random deacetylation on the chain. However, when sodium hydroxide solution is below 33%, the alkali is not penetrating α -chitin,⁶ leaving the crystal interior intact. Thus one can selectively deacetylate the crystalline surface⁷ without the acid hydrolysis. The glucosamine residues on the surface can be also selectively cleaved by periodate for further modifications.⁸

Other methods applied to cellulose can also be applied to chitin, namely sulfuric acid hydrolysis,⁹ tetramethylpiperidine-1-oxyl (TEMPO) catalyzed oxidation of primary alcohol on the surface.¹⁰ While N-deacetylation leads to cationic particles, other methods common to nanocellulose preparation leads to introduction of negative charge on the surface. The resulting nanochitin has zwitterionic character where the overall surface potential depends on the pH of the medium. Among these conventional methods, the sulfuric acid leads to the introduction of strong acidic group but with low density and accompanied by chain scission, while TEMPO oxidation leads to a high density of functional groups but of weakly acidic carboxyl groups. In this work, we aim to introduce high density of sulfate half-ester groups on the crystal surface.

Sulfation of cellulose in homogeneous conditions using different sulfation agent is reported,¹¹ among which sulfamic acid is relatively mild, and practical as the sulfamic acid itself is non-hygroscopic and stable solid. Sulfamic acid sulfation in N,N-dimethylformamide(DMF) has been also used to prepare long cellulose microfibril suspension without mechanical input.¹² In this work we tried to extend this method to crab-chitin to selectively modify nanochitin surface to modify its macroscopic behavior.

Experimental section

Materials

Commercially available ground chitin powder from crab shell was purchased from Golden-Shell Biochemical Co., Ltd (Zhejiang, China). They had typical particle size of about 20-100 μm . We further sequentially purified the sample by treating with 5% NaOH solution overnight followed by 12 hours treatment using 5% HCl under agitation at room temperature. After treatment with 4% H_2O_2 solution at pH=8, at 80 °C for 6 h, white powder was recovered by freeze-drying with macroscopic density of 0.36 g/cm^3 . The yield of this purification was about 80%. N,N-dimethylformamide (DMF, 99.5%) and sulfamic acid were purchased from Maclean Biochemical Technology Co., Ltd (Shanghai, China). Sodium hydroxide (NaOH, 99.7%), hydrochloric acid (HCl, 36-38%) and hydrogen peroxide (H_2O_2 , 30%) were purchased from Guanghua Sci-Tech Co., Ltd (Guangdong, China). The chemical reagents were used without further purification.

Nanochitin preparation

The typical sulfation medium for 1 g of chitin powder is 2.5 g of sulfamic acid dissolved in 50 mL DMF. The freeze-dried powder was put into the reaction medium heated at 80°C in an oil bath. We also varied the quantity of sulfamic acid, temperature and duration to study the reaction kinetics. The detailed reaction conditions were list in Table S1.

The reaction was terminated by vacuum filtration on a PTFE membrane (pore size = 0.2 μm) followed by washing with DMF by repeated resuspension and filtration to remove the excess sulfamic acid. Typically the operation was repeated 5 times with a 3-fold dilution with DMF. At each cycle we waited 10 minutes for the diffusion of unreacted sulfamic acid and side products from the powder. The filtrate remained a well-draining compact powder at this stage. The sample was then further washed by water to eliminate DMF. This was done by repeatedly suspending in deionized water followed by centrifugation at 7000 G for

10 minutes since the sample kept high amount of water that could not be drain through the filter. Three-fold dilution was repeated about 15 times until the pH of the supernatant remained neutral.

The water swollen powder was further diluted to 0.2% and dispersed by using high-pressure homogenizer passing through 200 μm zirconia nozzle at 80 MPa. This homogenization led to a translucent suspension that looks bluish under reflecting light. A scheme illustrating the preparation process is shown in Fig. 1.

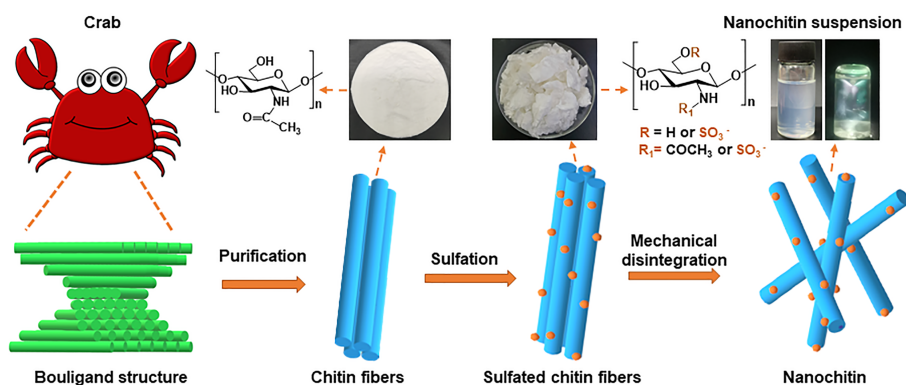


Fig. 1 Schematic illustration of heterogeneous sulfation of chitin. Crab chitin containing Bouligand structures, are purified as white powder, heterogeneously sulfated to keep the macroscopic aspect, but can be dispersed in to nanochitin by mechanical disruption.

Characterization

Optical microscopy The powder suspension was put on a glass slide and covered with a coverslip, and observed using polarizing microscope BX53M (Olympus, Japan), under crossed-polarizer and with insertion of a retardation plate.

Elemental analysis Carbon, hydrogen, nitrogen and sulfur contents were measured using elemental analyzer Vario EL cube (Elementar, Germany). The signal intensity was calibrated by using sulfanilamide to obtain the element weight fraction. Taking into account the oxygen in chitin and sulfated chitin, the sum of the weight fractions were 100% within 5% error.

Conductometric titration 20 mL of 0.2% chitin suspension was titrated with 10 mM NaOH, by adding at 0.1 mL step using a pipette. The total amount of NaOH added to achieve the minimum conductivity was used as equivalent of sulfate group in the system to deduce the degree of sulfation, assuming that all sulfate groups are in acid form before titration.

Infrared spectroscopy Freeze-dried powder was mixed to about 100:1 ratio with KBr, and finely ground to powder with mortar and pestle, and pressed into a pellet. The infrared absorption spectra was measured in transmission mode using infrared spectrometer (Bruker VERTEX 70, Germany).

X-ray diffraction Chitin powder or freeze-dried sulfated sample was spread in the groove of a glass sample holder and the excess was wiped off by the edge of a flat glass. The homogenized sample was freeze-dried to form aerogel, compacted between weighing paper by hand in form of a sheet and put on the sample holder so that the surface level coincides with the border. X-ray diffractometer (Bruker D8, Advance, Germany) with a Cu tube in line focus mode was operated at 40 kV and 30 mA in symmetric reflection geometry, and scanned with a scanning rate of $10^\circ/\text{min}$ (2θ).

Transmission electron microscopy (TEM) Nanofibers suspensions diluted to about 0.01 % was deposited onto a carbon membrane on a copper grid. Then 2% uranyl acetate drop was added, and waited for 90 seconds before removing the excess liquid by filtration paper tip. The sample was then dried overnight at room temperature, and then observed by using a transmission electron microscope (JEM-1400plus, Japan), operating at 90 kV. The fibril width was measured using ImageJ software taking the limit of white zone as the edge of the fibrils (Fig. S1).

Atomic force microscopy (AFM) Nanofibers suspensions diluted to about 0.01 % was deposited onto a freshly cleaved mica and dried at ambient temperature overnight. Observation was made using Dimension Icon (Bruker Billerica MA, Germany) in tapping mode.

Results and discussion

Infrared spectra and site of esterification

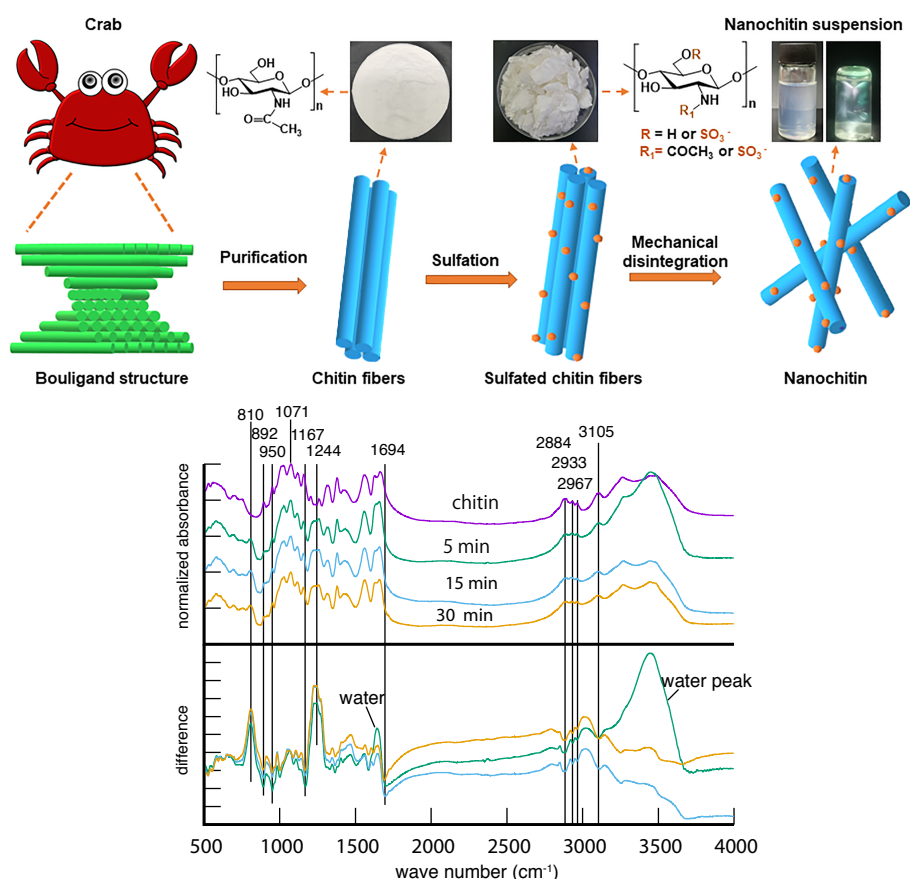


Fig. 2 Infrared spectra of chitin and sulfated nanochitin. Top: normalized to the absorbance at 1071 cm^{-1} and vertically shifted for clarity. Bottom: difference spectra subtracting the unreacted chitin spectra from sulfated chitin spectra. The time on the spectra indicates the duration of sulfation reaction at 80°C using 50 gL^{-1} sulfamic acid.

The chemical modification of chitin treated with 50 g/L sulfamic acid in DMF, in large excess, at 80°C as function of duration of reaction was observed in the Infrared spectra (Fig.

2). Their spectroscopic features are similar to untreated chitin, except that the new bands appeared at 804 cm^{-1} and 1240 cm^{-1} , They are characteristic to sulfate half-ester groups. In cellulose sodium sulfate, the corresponding peaks appear at 814 and 1260 cm^{-1} .¹³ Those peaks confirms that significant amount of sulfate groups indeed grafted on chitin.

In the difference spectra with respect to the pristine α -chitin (Fig. 2 bottom), we can also recognize the reduction of 892 cm^{-1} probably corresponding to the surface primary alcohol of the microfibril surface. In cellulose similar band is present at 897 cm^{-1} that is much less intense in thick microfibrils¹⁴ and is also negatively correlated to crystallinity,¹⁵ hence assigned to surface hydroxymethyl groups. This suggest that the O6 hydroxyl groups on the surface is modified.

A clear negative peak can also be seen on the higher wavelength limit of the amide I band at 1694 cm^{-1} . The position of the amide I band is highly correlated to hydrogen bonding, with isolated amide showing peaks at higher wavenumbers.¹⁶ Thus the negative difference peak at the higher wavenumber tail of amide I suggests the removal of surface acetamide groups. The decrease of the CH stretching peaks at around 2884 cm^{-1} appearing as negative peaks in the difference spectra is also corroborating with the surface deacetylation. The residual water might have contributed to deacetylation creating sites to form sulfamido groups.

Overall, the infrared spectroscopic data suggests that both O6 and N2 of the surface would be sulfated. Potentially O3 can be also sulfated, but the kinetic studies on cellulose indicates very low activity of O3 towards sulfation,^{11,17} and we do not see direct evidence of such O3 modification in the spectral features, although its possibility cannot be completely excluded.

Degree of sulfation

The general infrared features were consistent among different samples, but the sulfate peak intensity did not follow the reaction severity in the current measurement condition, and thus

could not be used to quantify the degree of sulfation. For the spectra to be quantitative in KBr method, the sample particles have to be ground to submicrometric sizes which might have not been the case, in the current manual grinding.

The elemental analysis data used for the degree of sulfation is given in table S1. The sulfate content can be estimated from elemental composition under different assumptions, using sulfur to carbon ratio, $r_{S/C}$ or sulfur to nitrogen ratio, $r_{S/N}$. One can consider two extreme cases: (1) N-acetyl groups are not partic as

$$DS_1 = 8r_{S/C}, \quad (1)$$

(2) only N-acetyl groups are reacting, thus each sulfation is accompanied by the removal of two carbon atoms and addition of one sulfur atom, leading to

$$DS_2 = \frac{8r_{S/C}}{1 + 2r_{S/C}}. \quad (2)$$

Also, if we consider that the number of N is not changing $DS_3=r_{S/N}$. The DS were summarized in Table S1.

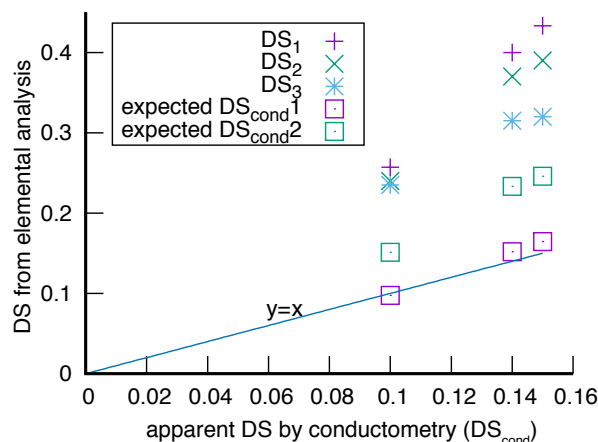


Fig. 3 Degree of sulfation estimated by elemental analysis and conductometric titration. The expected conductometric values depending on the fraction sulfate groups with ammonium counterion DS_{cond} (60% for DS_{cond1} and 40% for DS_{cond2}) are also plotted.

Conductometric titration is another way to estimate the degree of sulfation. As shown in Fig. S2, by neutralizing the highly mobile counter-ion, H^+ , with less mobile sodium ion, the conductivity of the suspension decreased until complete neutralization. Passed this neutralization, the conductivity increased again due to the highly mobile OH^- . The DS obtained by elemental analysis were plotted against DS from conductometric titration in Fig. 3, which shows linear correlation. However, the conductometric DS was systematically lower than the DS estimated from the elemental analysis by more than factor 2.

One reason for the discrepancy can be the existence of ammonium as counter-ion that contribute little to the conductivity. The presence of ammonium is also evidenced by the fact that the DS_3 estimated from sulfur to nitrogen ratio is systematically lower than the DS estimated from S/C ratio.

Since we do not have definitive information on the regio-selectivity of the surface sulfation of chitin, we consider the two extreme cases DS_1 and DS_2 . The fraction, r , of the sulfates with ammonium counterion can be estimated as

$$r = (DS_i - DS_3)/DS_i DS_3 \tag{3}$$

which were 0.6 for DS_1 and 0.4 for DS_2 . For a given DS, the conductometric titration should be actually measuring the remaining sites as

$$DS_{cond} = (1 - r)DS_i; \tag{4}$$

This expected titration taking into account the presence of ammonium counterion is plotted as "expected DS_{cond} " in Fig. 3. The scenario 1 is closest to the measured values, and is consistent to the general observation that O6 would be most susceptible to sulfation. Since infrared spectra also suggested some deacetylation, it is still not clear if primary alcohol is predominantly modified. Further analysis is required on the regio-selectivity of sulfation. We tentatively take the DS_1 as the degree of sulfation in the following discussion.

Kinetics of sulfation

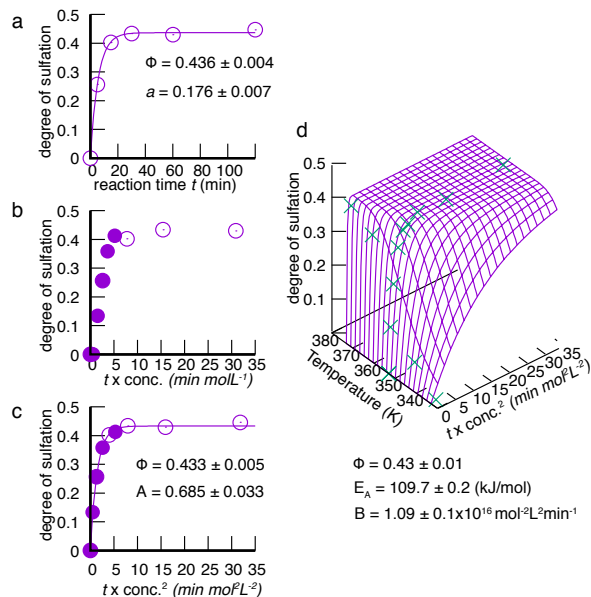


Fig. 4 Kinetics of sulfation. Degree of sulfation as function of a. reaction time with fixed sulfamic acid concentration of 0.5 molL^{-1} and temperature at $80 \text{ }^\circ\text{C}$. b. product of concentration and reaction time; filled circles are series with variable concentration. c. product of concentration squared and reaction time, d. both absolute temperature and c^2t with fit to a simple kinetic model (see text).

The kinetics of the sulfation can also be calculated from the DS. If we consider that a limited fraction of reactive groups are exposed to the sulfation reagent, and the sulfation reagent is in large excess, the reaction should follow first order-kinetics with respect to the available reactive groups, and degree of substitution will be expressed as

$$DS = \phi(1 - \exp(-at)) \quad (5)$$

where ϕ is the limit DS, a [min^{-1}] the kinetic constant and t [min] the duration of reaction. The DS calculated from elemental analysis indeed followed this curve (Fig. 4a). As the frequency of a molecule of sulfamic acid to encounter the reactive groups would scale with the concentration of sulfamic acid, one would expect a to be proportional to the concentration

$c[\text{molL}^{-1}]$, and thus

$$DS = \phi (1 - \exp(-bct)) \quad (6)$$

with a kinetic constant $b[\text{mol}^{-1}\text{Lmin}^{-1}]$. However, when we plot the DS including series with different sulfamic acid concentration, the curve does not superpose (Fig. 4b). Instead, if we plot DS against c^2t , all experimental data reacted at 80°C aligned on one line (Fig. 4c). This implies that probably two molecules of sulfamic acid are involved in the reaction, possibly through some intermediate. The experimental data could be fitted using the following function.

$$DS = \phi (1 - \exp(-Ac^2t)) \quad (7)$$

Finally we fitted the DS as function of temperature $T[\text{K}]$, t and c , assuming that there is one dominant activation energy E_A as

$$DS = \phi \left(1 - \exp \left(-Bc^2t \exp \left(\frac{-E_A}{RT} \right) \right) \right) \quad (8)$$

where R is the gas constant ($8.3 \text{ JK}^{-1}\text{mol}^{-1}$). The energy of activation E_A , the prefactor B and ϕ were fitted and shown in Fig. 4d. The activation energy of 109 kJ/mol is within the range of typical acetylation reactions of cellulose, which is reported to be between 40-70 kJ/mol in dissolving acetylation process,¹⁸ and 130 kJ/mol for heterogeneous acetylation of wood meal.¹⁹ The elemental analysis data used in the analysis is also given in table S1.

The limiting DS of 0.4 corresponds to a potential charge density of 2 mmol/kg since the mass of a monomer is 203 Da.

Anisotropic swelling in water

The swelling of the powder can be observed by a polarizing microscope. The initial apparent density of the starting chitin powder corresponds to a porosity of about 75% assuming the crystal density of 1.46 g/cm^3 ²⁰ before sulfamic acid treatment and washing with DMF

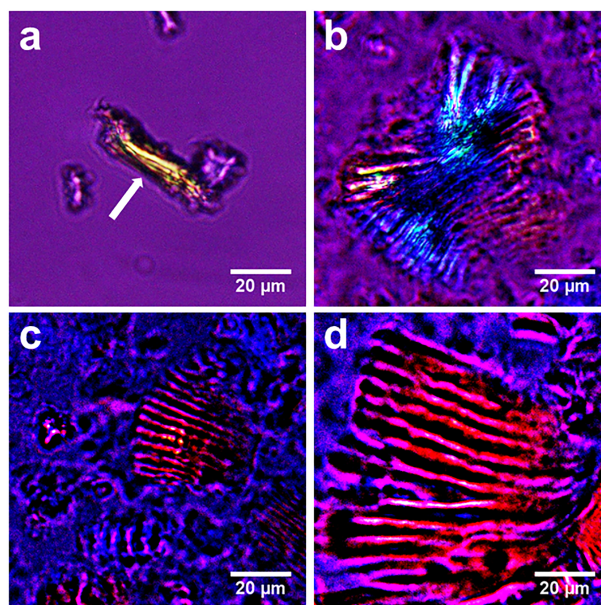


Fig. 5 Optical micrographs of water swollen chitin powders under crossed-polarizers with a retardation plate. a. pristine chitin powders, b. after 5 min sulfation, c. after 15 min sulfation, and d. after 30 min sulfation.

hardly increased the apparent volume. On the other hand, water was extensively swelling the structure. The swollen sulfated chitin powder was holding 16 to 25 times its dry weight even after centrifugation at 7000 G for 10 minutes. Contrary to the prolonged sulfation for algal cell wall,¹² chitin powder mostly kept its integrity, though at higher sulfation, part of the sample was lost probably because they detached as isolated fibrils from the fragment. The recovery of the centrifugation thus dropped to about 60% when the sulfation reaction was carried out for more than 1 hour in these conditions.

Fig. 5 and S3 show the optical micrographs of chitin powder in water before and after sulfation process. Most of the unmodified chitin powder particles showed little birefringence probably because the relatively flat flakes where fragments were parallel to the exoskeleton plane. The chitin microfibrils (and thus the chains) are running in all directions due to the helical structure. Only fragments that happened to be upright show strong birefringence (Fig. 5a arrow head). When sulfated powder is swollen in water, the particles show periodic stripes of birefringent region that shows up bright under crossed-polarizers at 45° with respect to the polarizing direction (Figure S3). Insertion of a retardation plate of 530 nm shows the

yellow and blue color of the stripes depending on the orientation of the stripe. This is due to the birefringence of chitin²¹ and the helicoidal structure of crab exoskeletons.^{22,23} Dark zone corresponds to the region where the chitin chains points to the direction of observation.

The fact that we observe more fragments showing this stripe pattern in the highly swollen particles after sulfation suggests a highly anisotropic swelling inverting the aspect ratio of the particle, probably transforming the oblate fragments into prolate form where the long axis is now in the helical direction, thus lay parallel to the glass slide. We observe a typical half pitch of 4–5 μm . The chiral half-pitch of crab exoskeleton is reported to be predominantly slightly smaller than 1 μm ²³ and thus it would suggest that the swelling along the helical axis is around 5 times. As the volume swelling was 16–25 times, the cross-sectional area would have swollen by 4–5 times. This corresponds to 2–2.5 times expansion in each direction. This situation happens if the interfibrillar distances are multiplied by 5 in a helicoidal organization.

How the structure is still maintaining the integrity in this highly swollen situation is not clear, but since they are only loosely held together a simple mechanical homogenization completely disrupt the integrity as seen below.

Nanochitin dispersion

The nanodispersion after homogenization can be directly inspected by eyes as slightly bluish aspect in reflection and yellow-reddish impression in transmission. This visual inspection already tells that suspension should contain fine scattering elements with dimensions smaller than the wavelength of visible light.

To further obtain idea on the dimension of the suspending particles, we analyzed the transmission spectra as turbidity, assuming that the attenuation of the transmitted light is only due to scattering. For nano-fibrils, we are expecting a power law of turbidity following λ^{-3} , where λ is wavelength of light.²⁴

The wavelength dependence of the suspension was not as steep as expected for a nano-fibrils, and followed roughly λ^{-1} (Fig. 6). After centrifugation at 10 000 G for 15 min,

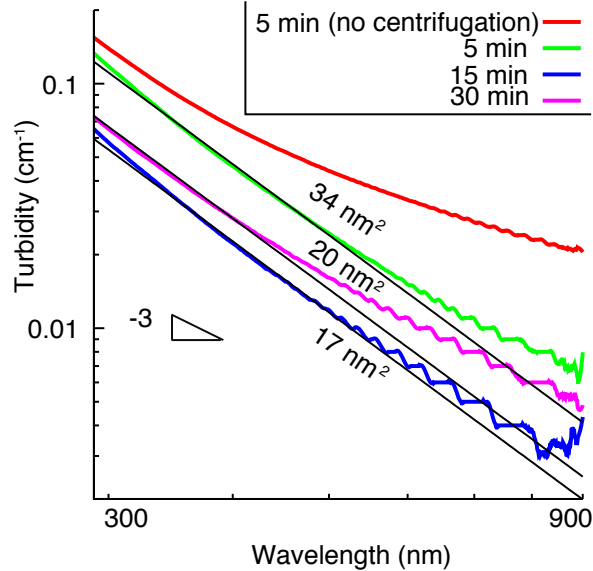


Fig. 6 Turbidity of chitin suspensions as function of wavelength. The minutes on the legend indicates the duration of sulfation reaction at 80°C. Straight lines are theoretical lines for infinite long fibrils of indicated the cross-sectional area.

small amount of sediment (4% of dry material) was observed, and the supernatant showed a turbidity that follows wavelength dependence proportional to λ^{-3} (Fig 6), signature of elongated objects whose lateral dimensions are much smaller than the wavelength of visible light.^{24,25} Thus, the major part of the sample could be dispersed as nanofibrils.

To determine the lateral dimension of the nanofibrils, we need the refractive index of the particles. The reported refractive indices for chitin ranges from 1.52 to 1.6,²⁶⁻²⁸ but they are in general the macroscopic refractive index including the voids and thus are lower bound for the intrinsic refractive index of α chitin. Using the crystal density $\rho_c = 1.46 \text{ g/cm}^3$ of α chitin,²⁰ refractive index of chitin 1.6, and of water $\rho_w = 1.333$ the $dn/dc = (\rho_c - \rho_w)/1.6 = 0.184$. we can roughly estimate the cross-sectional area of fibrillar objects evolving from 34 nm² to 17 nm² according to the turbidity data (calculation detail in SI). If we take the lower bound of refractive index, 1.52, the $dn/dc = 0.13$ and the estimated cross-sectional area would be doubled.

While the pH of the sample suspension before homogenization was between 6 and 7, it went down to 3.86 after homogenization indicating that the proton from the surface of the

nanochitin were now found in the bulk. Those protons had been probably entrapped in the submillimetric powder gel before homogenization leading to higher apparent pH. The fact that chitin powder keeps its integrity during the sulfation and washing is interesting from processing point of view, as there is no increase in viscosity of reaction mixture, and also facilitates washing of the final product by allowing easy exchange with fresh solvent. This is an advantage compared to sulfuric acid hydrolysis for example, where the sample cannot be easily recovered by centrifugation and the final removal of electrolytes are usually done by long dialysis.

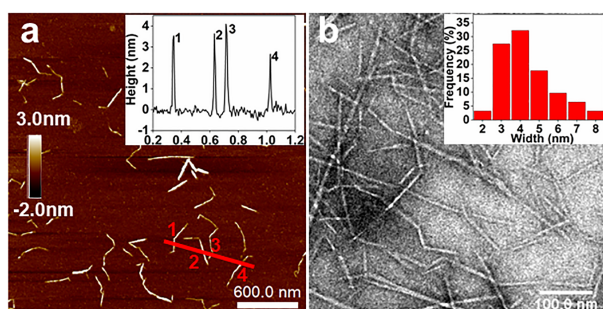


Fig. 7 Micrographs of nanochitin after 5 min sulfation at 80 °C. a. AFM image of nanochitin deposited on mica surface, with insert height profile along the red line in the image. b. Negative stain transmission electron micrographs with width histogram in the insert.

The specific morphology of nanochitin was obtained by AFM and TEM. When further diluted in water and deposited on freshly cleaved mica or on carbon grid, we observed typical height of the order of 3 - 4 nm by AFM and width of 3 - 5 nm by negative staining TEM, while the lengths of straight segments were a few hundred nanometers (Fig. 7). The straight segments seem to be linked through kink to make a fibril with contour length of 0.5 - 1 μm length. As shown in Fig. S4, nanochitin after 15 and 30 minutes treatment exhibited similar morphology. The kinks are probably due to the mechanical treatment as is in the case of cellulose nanofibrils.²⁹

The crystalline structure and size can be determined by the X-ray diffraction. As shown in Fig. 8, the samples both after sulfation and homogenization both showed the same crystalline structure but with broader line width indicating smaller crystallite width. Sulfation alone

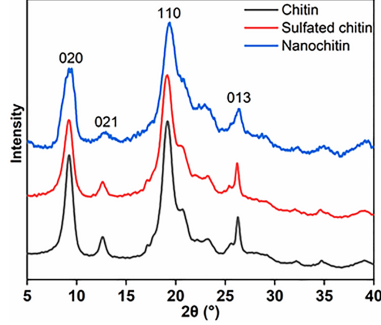


Fig. 8 X-ray diffraction profiles of chitin and nanochitin. Sulfation was done at 80°C using 50 gL⁻¹ sulfamic acid for 5 minutes.

broadened the line slightly, and the homogenization enhanced this tendency (Fig. 8, Fig. S5). Since there is no loss in the amount of sample, this decrease in size should be the result of splitting. The Scherrer size based on 0 2 0 reflection decreased from 8.2 nm to 6.5 nm by sulfation, and further down to 5.5 nm by the following homogenization (Table S2). Still this size is significantly larger than the particles observed under TEM or AFM (3-4 nm). This is because X-ray diffraction and turbidity represent the volume average of the lateral size, and the larger particles, though small in number, is representing a larger volume in the system.

Both X-ray diffraction line-broadening and turbidimetric measurement is representing roughly the weight average of the particle size. On the other hand, microscopic technique rather tends to focus on smaller objects, and give impression of smaller size. Still all measurement fell in the range between 3 - 6 nm thickness. The sulfamic acid treatment in DMF has an effect similar to TEMPO oxidation on cellulose in that it preferentially brings charge on the surface than hydrolyzing the chain. The preservation of long fibrillar nature probably allows more efficient transmission of external mechanical force to split the lateral aggregates into single crystalline elements, and hence leads to monodisperse lateral dimension.

Given the lateral dimension and DS, the potential linear charge density or surface charge density can be estimated. The unit cell of α -chitin has a volume, of 0.927 [nm³]³⁰ and contains 4 residues, so the volumic charge density $\rho_v = 4 \text{ DS} / 0.927 \text{ [nm}^{-3}\text{]}$. If we assume a circular cross-section with a diameter of D nm, linear charge density ρ_l can be obtained just by multiplying ρ_v with the cross-sectional area, $\pi D^2/4$. Similarly, the surface charge density

ρ_s can be obtained by multiplying with volume to surface ratio $4/D$. The limit DS of 0.4 and diameter of 5 nm leads to $\rho_l = 34 \text{ [nm}^{-1}\text{]}$ and $\rho_s = 1.38 \text{ [nm}^{-2}\text{]}$.

Probably conceptually the most closest nanochitin to the one obtained here is the sodium-hydroxide deacetylated nanofibrils by Fan et al.⁷ Although TEMPO oxidation in cellulose leads to a very long individualized microfibril suspensions,^{31,32} the same treatment on chitin^{10,33} tended to keep bundles with significant fragmentation in length. The limiting degree of deacetylation in the former case was about 0.3 to 0.4, similar to our maximum DS. The sum of carboxyl and aldehyde groups introduced by TEMPO oxidation levelled off at 1 mol/kg,¹⁰ about half of the sulfate groups in our case. One possible interpretation is that the sulfation predominantly occurs at O6, so the same number of residues exposes the O6 to sulfation in our case as does the N-acetyl groups in the alkali deacetylation. The bundling of chitin in the TEMPO reaction medium might have limited the number of exposed primary alcohol to about half of what is exposed in our sulfating media.

Conclusion

We demonstrated that heterogeneous sulfation, selectively sulfating the microfibril surface of crab-chitin, can be achieved using sulfamic acid as sulfating agent in a polar aprotic solvent DMF. The sulfated chitin maintained its integrity up to a bulk DS of 0.4 when gently handled, but could be dispersed in to nanofibrils by high-pressure homogenization. The kinetics of sulfation followed first-order to the available reaction site, and second order to the sulfamic acid. This approach allows a well controlled selective sulfation for the preparation of nanochitin elements.

Acknowledgement

We are indebted to staffs of Analytical and Testing Center of SCUT: Dr. Andi Wang for XRD measurement, Dr Qingyou Liang and Dr. Shenghui Zeng for infrared spectroscopy.

We also thank colleagues from SCUT/State key laboratory of Pulp and Paper engineering: Dr. Weiyang Li for elemental analysis, Dr Yanbo Huang for the assistance in AFM observations and Shanyong Wang for help in polarized optical microscopy. Dr. Jean-Luc Putaux of CERMAV, France for the preliminary TEM observation of sulfated chitin nanoparticles and NanoBio-ICMG Platform (UAR 2607, Grenoble) for granting access to the Electron Microscopy facility. The transmission electron microscopy in this article was carried out by Shiyanjia Lab (www.shiyanjia.com). The work was financially supported by the National Natural Science Foundation of China (21774036), Guangdong Province Science Foundation (2017GC010429) and Science and Technology Program of Guangzhou (202002030329).

Supporting Information Available

Calculation detail of the cross-section calculation from the turbidimetry data, conductometric titration curves, polarized optical micrographs without retardation plate, atomic force micrographs of nanochitin sulfated for 15 minutes and 30 minutes at 80°C, X-ray diffraction profiles of sulfated chitin, nanochitin and its corresponding Scherrer size, primary data of elemental analysis are provided in the supporting information file.

References

- (1) Marchessault, R. H.; Morehead, P. P.; Walter, N. M. Liquid crystal system from Fibrillar Polysaccharides. *Nature* **1959**, *184*, 632–633.
- (2) Revol, J. F.; Marchessault, R. H. In vitro chiral nematic ordering of chitin crystallites. *Int. J. Biol. Macromol.* **1993**, *15*, 329–335.
- (3) Belamie, E.; Davidson, P.; Giraud-Guille, M. M. Structure and Chirality of the Nematic Phase in α -Chitin Suspensions. *J. Phys. Chem. B* **2004**, *108*, 14991–15000.

- (4) Escott, G. M.; Adams, D. J. Chitinase Activity in Human Serum and Leukocytes. *Infection and Immunity* **1995**, *65*, 4770–4773.
- (5) Goodrich, J. D.; Winter, W. T. α -Chitin Nanocrystals Prepared from Shrimp Shell and Their Specific Surface Area Measurement. *Biomacromolecules* **2007**, *8*, 252–257.
- (6) Thor, C. H. B.; Henderson, W. F. Alkali Chitin. *American Dyestuff Reporter* **1940**, *29*, 461–464.
- (7) Fan, Y.; Saito, T.; Isogai, A. Individual Chitin Nano-whiskers Prepared from Partially Deacetylated α -Chitin by Fibril Surface Cationization. *Carbohydr. Polym.* **2010**, *79*, 1046–1051.
- (8) Liu, P.; Liu, H.; Schäfer, T.; Gutman, T.; Gibhardt, H.; Qi, H.; Tian, L.; Zhang, X. C.; Buntkowsky, G.; Zhang, K. Unexpected Selective Alkaline Periodate Oxidation of Chitin for the Isolation of Chitin Nanocrystals. *Green Chemistry* **2021**, *23*, 745–751.
- (9) Huang, Y.; Yao, M.; Zheng, X.; Liang, X.; Su, X.; Zhang, Y.; Lu, A.; ; Zhang, L. Effects of Chitin Whiskers on Physical Properties and Osteoblast Culture of Alginate Based Nanocomposite Hydrogels. *Biomacromolecules* **2015**, *16*, 3499–1507.
- (10) Fan, Y.; Saito, T.; Isogai, A. Chitin Nanocrystals Prepared by TEMPO-Mediated Oxidation of α -Chitin. *Biomacromolecules* **2008**, *9*, 192–198.
- (11) Wagenknecht, W.; Nehls, I.; Köts, J.; Philipp, B.; Ludwig, J. Untersuchungen zur Sulfatierung teilsubstituierter Celluloseacetate unter homogenen Reaktions Bedingungen. *Cellul. Chem. Technol.* **1991**, *25*, 343–354.
- (12) Briois, B.; Saito, T.; Pétrier, C.; Putaux, J.-L.; Nishiyama, Y.; Heux, L.; Molina-Boisseau, S. $I_\alpha \rightarrow I_\beta$ Transition of Cellulose under Ultrasonic Radiation. *Cellulose* **2013**, *20*, 597–603.

- (13) Chen, G.; Zhang, B.; Zhao, J.; Chen, H. Improved Process for the Production of Cellulose Sulfate using Sulfuric Acid/Ethanol Solution. *Carbohydr. Polym.* **2013**, *95*, 332–337.
- (14) Åkerholm, M.; Hinterstoisser, B.; Salmén, L. Characterization of the Crystalline Structure of Cellulose using Static and Dynamic FT-IR Spectroscopy. *Carbohydr. Res.* **2004**, *339*, 569–578.
- (15) Nelson, M. L.; O'Connor, R. T. Relation of Certain Infrared Bands to Cellulose Crystallinity and Crystal Lattice Type. Part I. Spectra of Lattice Types I, II, III and of Amorphous Cellulose. *Journal of Applied Polymer Science* **1964**, *8*, 1311–1324.
- (16) Torii, H.; Tatsumi, T.; Kanazawa, T.; Tasumi, M. Effect of Intermolecular Hydrogen-Bonding Interactions on the Amide I Mode of N-Methylacetamide: Matrix-Isolation Infrared Studies and ab Initio Molecular Orbital Calculations. *J. Phys. Chem. B* **1998**, *102*, 309–314.
- (17) Wagenknecht, W.; Nehls, I.; Philipp, B. Studies on the Regioselectivity of Cellulose Sulfation in an N₂O₂-N,N-Dimethylformamide-Cellulose System. *Carbohydr. Res* **1993**, *240*, 245–252.
- (18) Luo, P.; Cao, C.; Liang, Y.; Ma, X.; Xin, C.; Jiao, Z.; Cao, J.; Zhang, J. Kinetic Study of the Acetylation of Cotton Linter Pulp. *BioResources* **2013**, *8*, 2708–2718.
- (19) Minato, K.; Ito, Y. Analysis of the Factors Influencing the Acetylation Rate of Wood. *Journal of Wood Science* **2004**, *50*, 519–523.
- (20) Minke, R.; Blackwell, J. The Structure of α -Chitin. *J. Mol Biol* **1978**, *120*, 167–181.
- (21) Castle, E. S. The Double Refraction of Chitin. *Journal of General Physiology* **1936**, *19*, 797–805.
- (22) Bouligand, Y. Sur une Architecture Torsadée Répandue dans de Nombreuses Cuticules

- d'Arthropodes. *Compte Rendues Hebdomadaire des séances de l'Académie des sciences* **1965**, *261*, 3665–3668.
- (23) Giraud-Guille, M.-M. Fine Structure of the Chitin-Protein System in the Crab Cuticle. *Tissue & Cell* **1984**, *16*, 75–92.
- (24) Carr Jr., M. E.; Hermans, J. Size and Density of Fibrin Fibers from Turbidity. *Macromolecules* **1978**, *11*, 46–50.
- (25) Tanaka, R.; Kuribayashi, T.; Ogawa, Y.; Saito, T.; Isogai, A.; Nishiyama, Y. Ensemble Evaluation of Polyisperse Nanocellulose Dimensions: Rheology, Electron microscopy, X-ray Scattering and Turbidimetry. *Cellulose* **2017**, *24*, 3231–3242.
- (26) Becking, L. B.; Chamberlin, J. C. A note on the Refractive Index of Chitin. *Proceedings of the Society for Experimental Biology and Medicine* **1925**, *22*, 256.
- (27) Azofeifa, D. E.; Arguedas, H. J.; Vargas, W. E. Optical Properties of Chitin and Chitosan Biopolymers with Application to Structural Color Analysis. *Optical Materials* **2012**, *35*, 175–183.
- (28) Leertouwer, H. L.; Wilts, B. D.; Stavenga, D. G. Refractive Index and Dispersion of Butterfly Chitin and Bird Keratin Measured by Polarizing Interference Microscopy. *Optics Express* **2011**, *24*, 24061–24066.
- (29) Usov, I.; Nyström, G.; Adamcik, J.; Handschein, S.; Schütz, C.; Fall, A.; Bergström, L.; Mezzenga, R. Understanding Nanocellulose Chirality and Structure-Properties Relationship at the Single Fibril Level. *Nature Communications* **2015**, *6*, 7564.
- (30) Sikorski, P.; Hori, R.; Wada, M. Revisit of α -Chitin Crystal Structure using High Resolution X-ray Diffraction Data. *Biomacromolecules* **2009**, *10*, 1100–1105.

- (31) Saito, T.; Nishiyama, Y.; Putaux, J. L.; Vignon, M.; Isogai, A. Homogeneous suspensions of individualized microfibrils from TEMPO-catalyzed oxidation of native cellulose. *Biomacromolecules* **2006**, *7*, 1687–1691.
- (32) Saito, T.; Kimura, S.; Nishiyama, Y.; Isogai, A. Cellulose nanofibers prepared by TEMPO-mediated oxidation of native cellulose. *Biomacromolecules* **2007**, *8*, 2485–2491.
- (33) Jiang, J.; Ye, W.; Yu, J.; Fan, Y.; Ono, Y.; Saito, T.; Isogai, A. Chitin Nanocrystals Prepared by Oxidation of *alpha*-Chitin Using the O₂/Laccase/ TEMPO system. *Carbohydr. Polym.* **2018**, *189*, 178–183.

TOC Graphic

